

Semi-analytical approaches to study hot electrons in the shock ignition regime

M. Afshari,^{1, a)} L. Antonelli,² F. Barbato,³ G. Folpini,³ K. Jakubowska,⁴ E. Krousky,⁵ O. Renner,⁶ M. Smid,⁶ and D. Batani³

¹⁾ *GSI Helmholtzzentrum für Schwerionenforschung GmbH, Planckstraße 1, 64291 Darmstadt, Germany*

²⁾ *Department of Physics, University of York, YO10 5DD York, England*

³⁾ *Universite Bordeaux, CNRS, CEA, CELIA, UMR 5107, F-33405 Talence, France*

⁴⁾ *Institute of Plasma Physics and Laser Microfusion, IPPLM, 01-497 Warsaw, Poland*

⁵⁾ *Institute of Plasma Physics CAS, v.v.i., 1782/3 182 00 Prague, Czech Republic*

⁶⁾ *Institute of Physics of ASCR, v.v.i., 1999/2 182 21 Prague, Czech Republic*

(Dated: 15 November 2018)

Hot electrons role in shock generation and energy deposition to hot dense core is crucial for the shock ignition scheme implying the need for their characterization at laser intensities of interest for shock ignition. In this paper we analyze the experimental results obtained at the PALS laboratory and provide an estimation of hot electrons temperature and conversion efficiency using a semi analytical approach, including Harrach-Kidder's model.

Keywords: Shock ignition; Hot electron; Harrach-Kidder's model

I. INTRODUCTION

By increasing the gain and mitigating the constraints on the target fabrication and irradiation uniformity, the Shock Ignition (SI) approach to inertial confinement fusion¹ should allow achieving nuclear ignition with current laser facilities^{2,3}. In spite of such advantages, there are still many unresolved issues concerning the physics of shock ignition. One of the most important topics is the effect of parametric instabilities. They not only reduce the coupling of laser energy to the plasma (reflection of incident laser light), resulting in lower shock pressure, but can also accelerate a fraction of electrons to high energies creating Hot Electrons (HE)^{4,5}.

HE have equivocal effect in SI: if their energies are higher than ≈ 100 keV, they can preheat the fuel making its compression more difficult and finally can prevent ignition. On the other hand, if they have energies below ≈ 100 keV, they are unable to penetrate to the denser part of the target, and they may turn to be a positive factor by increasing laser-target coupling and shock pressure⁶. Laser plasma interaction produces HE by different physical mechanisms such as SRS (Stimulated Raman Scattering), TPD (Two Plasmon decay) and resonant absorption. All of them produce non mono-energetic electrons characterized by a distribution in energy $f(E)$ and hence a hot electron temperature, T_{HE} . The energy conversion and HE temperature are critical parameters in order to evaluate the positive vs. negative effects of HE in SI.

In order to study the physics of HE generation in an intensity regime relevant to SI, we performed an experiment at the Prague Asterix Laser System laboratory, PALS in Prague Czech republic. One of the goals of the experiment was the study of generation and propagation of HE and their role in shock wave generation⁶. The objective of this paper is the

^{a)}Electronic mail: m.afshari@gsi.de

analysis of the experimental results with semi-analytical approaches, in particular Harrach-Kidder's model⁷. This model is particularly adapted to describe the propagation of HE in the target when HE energy is not high and therefore the motion of electrons become quickly isotropic due to collisions in the target. Although Monte-Carlo simulations are a powerful tool for analyzing data on HE dynamics, nevertheless the use of semi-analytical models may represent a quick alternative for estimating the parameters of HE distribution, with the advantage of suggesting information on the physical mechanisms at play.

The paper is organized as follow: Sec.2 contains the set-up of the experiment. The analysis of raw X-ray images to determine the $K\alpha$ spot size and the total number of emitted $K\alpha$ photons are illustrated in Sec.3. In Sec.4 we present the experimental results and compare the characteristic of HE emitted at $1\omega/3\omega$ laser frequencies. In Sec.5 we estimate the HE energy first by calculating the range and relating it to HE energy using the ESTAR database⁸ and then with the semi-analytical model developed by Harrach & Kidder. Sec.6 contains the conclusions.

II. EXPERIMENT SET-UP AND DIAGNOSTIC

In this Section we describe the set-up and the diagnostics. In the experiment we used two laser beams. The first one is the PALS main laser beam operating either at 1ω or 3ω harmonics ($\lambda=1315$ nm/438 nm, maximum energy 440/170J, pulse duration 300 ps) focused onto the target with $100\mu\text{m}$ focal spot. The intensity of the main laser pulse was varied by changing the laser pulse energy, whereas pulse duration and focal spot size were kept fixed throughout the experiment. The maximum available intensity was 2×10^{16} W/cm² at 1ω and 9×10^{15} W/cm² at 3ω . The second beam, used on some shots, was an auxiliary beam ($\lambda=1315$ nm at 1ω , energy up to 100 J, pulse duration 300 ps, $I \approx 10^{14}$ W/cm²) focused onto the target with the Gaussian focal spot ($\approx 300\mu\text{m}$) incident at 30° from target normal in the vertical direction. For the auxiliary beam we chose 1ω irradiation because in this case the laser beam generates a plasma with higher temperature at the critical surface in comparison to plasma produced at 3ω . In this way we tried to compensate the low energy available in the beam. The main pulse irradiated the target after the auxiliary beam with delays $t = 0, 300, 600$ and 1200 ps. In fact the auxiliary beam creates a long-scale plasma (preplasma) and then the main laser pulse at 1ω or 3ω focused inside the preplasma produces the HE beam and launches a shock wave.

To ensure a better focal spot uniformity, phase plates were used on both beams. On a few shots at 3ω , the phase plate on the main beam was removed to reach higher intensities (up to 3×10^{16} W/cm²) in a focal spot with the average diameter $\approx 60\mu\text{m}$.

During the experiment we used different targets but two types of targets were dedicated specifically to HE studies. The first type of targets were thin multilayer targets: CHCl-Ti-Cu. The first layer was a Chlorinated plastic (Parylene-C, $\text{C}_8\text{H}_7\text{Cl}$) with different thicknesses (3-10-25 μm). The CHCl layer was followed by two thin layers of high Z material (Ti, Cu) used as traces layers for the fluorescence emission resulting from the interaction of HE. The second type of targets were thick Cu targets either bare or coated with a CHCl layer on the laser side with thicknesses 25 and 40 μm . The thick Cu layers exclude the possibility of HE refluxing. Fig.1 shows a schematic of targets.

To characterize the HE generation in the plasma we used spherically bent crystals to image the $K\alpha$ spot onto the X-ray films⁹. Fig.2 shows the experiment setup and a typical image of the X-ray film. The films used in our experiment (Kodak Industrex \times AA400 film) are calibrated¹⁰. Images (Fig.2, right) show the geometry of the $K\alpha$ spot and hence the geometry of the HE beam crossing the Ti/Cu layers. They also allow to extract the total number of $K\alpha$ photons which irradiated the film. To estimate the total number of $K\alpha$ photons emitted from the target on 4π , we multiply the total number of $K\alpha$ photons detected on the X-ray film by the transfer characteristics of the imaging system, ζ

$$\zeta = \frac{4\pi}{RT\Omega} \quad (1)$$

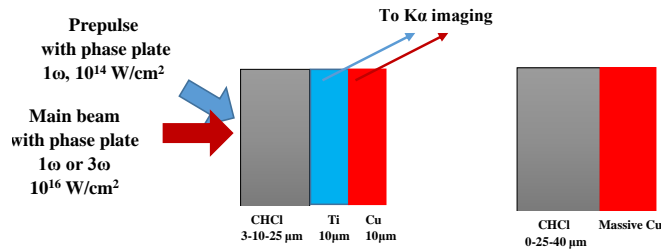


FIG. 1. Schematic view of the thin multilayer targets (left) and thick Cu targets (right).

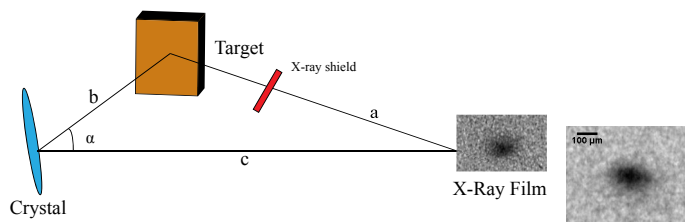


FIG. 2. Left: Set up for Kα imaging measurement. The X-ray shield protects the X-ray film from direct irradiation of the target. The distances of Target-Film (a), Target-Crystal (b) and Crystal-Film (c) are 22 cm, 30 cm and 51.9 cm respectively. The magnification of the system is $M=1.73$.

Right: Typical Cu Kα spot (black spot) as recorded on the X-ray film.

where

- R is Integrated reflectivity of the crystal, which for Cu is $R_{Cu}=47.02 \mu\text{rad}$ at wavelength 1.5406 \AA and for Ti is $R_{Ti}=906.0 \mu\text{rad}$ at wavelength 2.748 \AA .
- T is the transition of the filters placed before the X-ray film, $60 \mu\text{m Al} + 20 \mu\text{m mylar}$. The overall transmission of Kα through these filters for Cu is $T_{Cu}=0.45$ and for Ti is $T_{Ti}=0.014$.
- Ω is the collection solid angle given by $\Omega = \frac{S \sin(\theta_\beta)}{b^2}$ where S is the area of the crystal surface (the radius of the crystal surface is 1.2 cm), θ_β is the Bragg angle of the crystal (88.15°) and b is the target-crystal distance (30cm).

Taking into consideration all above parameters, the transfer characteristics of the imaging system is estimated to be $\zeta_{Cu}=5.2 \times 10^5$ for Cu and $\zeta_{Ti}=1.6 \times 10^6$ for Ti. For instance, this implies that one Cu Kα photon collected on the X-Ray film corresponds to 5.2×10^5 photons emitted from the target in 4π .

We have to mention the coronal x-ray emissions, which are the bremsstrahlung emissions of electrons from the tail of electron distribution in the corona with energy above the Kα emission, should be very negligible in comparison to the x-ray emissions due to the interaction of HEs with the target. The Cu Kα pumping by coronal x-rays has been analyzed in previous studies¹¹ where for analogous experimental conditions it was demonstrated that even at uncoated Cu targets, where the coronal temperature is rather high ($\leq 2 \text{ keV}$, as determined experimentally and supported by Multi-2D hydrodynamic modeling¹²), the K-shell excitation due to the corona radiation can be neglected, being at the level of 5% compared to the effect of HEs with the characteristic temperature of 30 keV. At the same time, the coronal temperature at plastic coated targets is much lower, typically at the level of 700 eV¹³, i.e. the effect of K-shell pumping due to the coronal emission is still smaller. We note that the contribution of HE induced continuum is much weaker in comparison

to the action of coronal radiation, thus the K-shell excitation is governed by HEs and the effects of radiation originating from the laser matter interaction can be neglected.

III. EXPERIMENTAL RESULTS

We studied the variation of the $K\alpha$ spot size and the $K\alpha$ photon numbers as a function of:

- Energy of main laser beam;
- Preplasma (energy of auxiliary laser beam and delay between the two beams);
- Thickness of the plastic layer before the tracers (Cu and Ti);

A. Measurements of $K\alpha$ Spot size vs. Laser Energy

To determine the effect of the laser energy on $K\alpha$ spot size, we plot the $K\alpha$ spot sizes of thin targets vs. the laser energy for both $1\omega/3\omega$ frequencies (Fig.3).

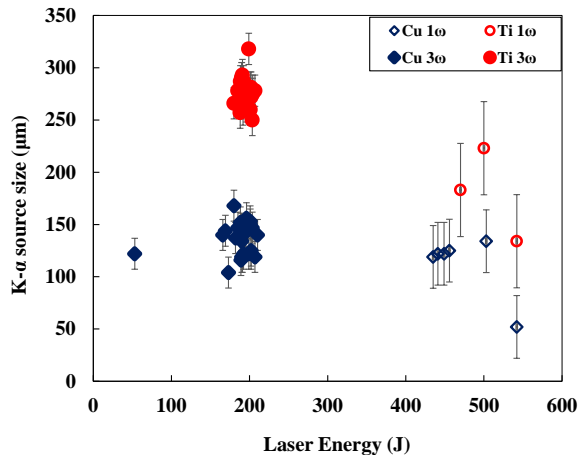


FIG. 3. $K\alpha$ spot size vs. main laser energy for thin multilayer targets.

On average the size of the Cu $K\alpha$ spot is $\approx 130\mu\text{m}$ which is about 1.3 times the size of the focal spot. As we can see the Cu $K\alpha$ spot size is comparable at both $1\omega/3\omega$ frequencies. The Ti $K\alpha$ spot size is bigger than the Cu one at both $1\omega/3\omega$ frequencies, typically a factor 1.5-3. This might at first seem strange because one can expect the size to increase with depth, due to the divergence of HE in the target. Nevertheless it has to be considered that the Cu is the third layer and that Cu $K\alpha$ emission (8027 eV) is more energetic than Ti $K\alpha$ emission (4504 eV). Hence only the more energetic electrons can reach the Cu layer and excite it and these more energetic electrons are probably emitted with lower angular divergence.

B. Measurement of $K\alpha$ photons vs. Laser Energy

The variation of the number of Cu and Ti $K\alpha$ photons emitted over the whole solid angle, 4π , for thin targets is plotted versus laser energy for both $1\omega/3\omega$ frequencies in Fig. 4. On average the number of $K\alpha$ photons emitted over 4π are: $(1 \pm 0.5) \times 10^{12}$ for Ti at 3ω , $(4 \pm 1) \times 10^{11}$ for Ti at 1ω , $(1 \pm 0.2) \times 10^{11}$ for Cu at 3ω , and $(5 \pm 4) \times 10^{10}$ for Cu at 1ω .

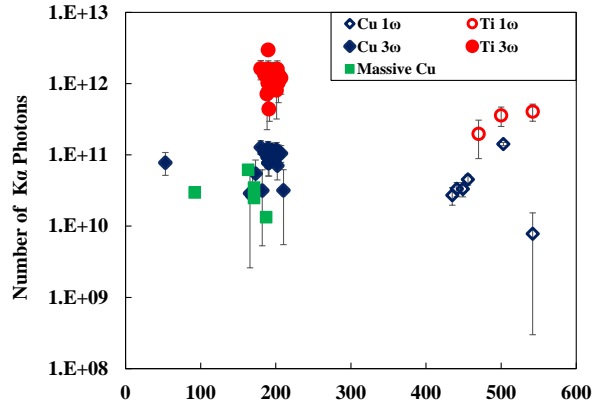


FIG. 4. Number of $K\alpha$ photons versus main laser energy for thin targets at both $1\omega/3\omega$ frequencies and thick Cu targets at 3ω frequency.

As expected the number of Ti $K\alpha$ photons is higher than the number of Cu $K\alpha$ photons at both 1ω and 3ω . Indeed Ti is the second layer (therefore more HE arrive there in comparison to the Cu layer) and also Ti $K\alpha$ is excited at lower energies.

Fig.4 also shows the variation of the number of emitted Cu $K\alpha$ photons for thick Cu targets at 3ω . The smallest number of Cu $K\alpha$ photons is obtained with the thick Cu targets with plastic over layer. This seems to point out to some effects of HE refluxing in the thin targets (effect which is of course not present in the thick targets).

C. Study of the Effect of Preplasma on $K\alpha$ Spot size and $K\alpha$ intensity

To show the effect of preplasma on $K\alpha$ spot size we divided the data into two groups, with and without preplasma. We have plotted in Fig.5 the variation of the $K\alpha$ spot size for these two groups versus laser energy at both $1\omega/3\omega$ for thin targets.

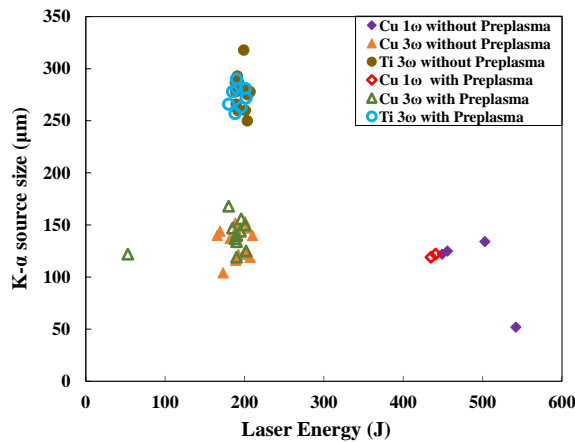


FIG. 5. Effect of preplasma on $K\alpha$ spot size for thin targets at both $1\omega/3\omega$ frequencies.

As we can see all $K\alpha$ spots with or without preplasma have approximately the same size, showing that the preplasma has no appreciable effect on the $K\alpha$ spot size at both $1\omega/3\omega$ frequencies.

To check the effect of preplasma on the number of $K\alpha$ photons we plotted in Fig.6 the variation of $K\alpha$ photon numbers vs. the laser energy at both $1\omega/3\omega$ for thin targets with

and without preplasma.

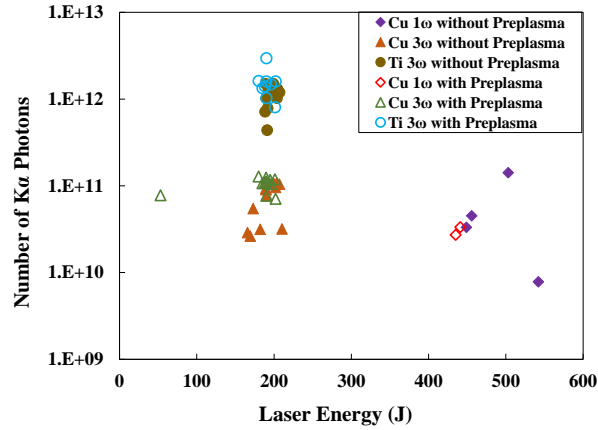


FIG. 6. Effect of preplasma on the number of $K\alpha$ photons for thin targets at both $1\omega/3\omega$ frequencies.

Again, the preplasma seems to have no main effect on $K\alpha$ emission.

D. Study of the effect of plastic thickness on $K\alpha$ emissions

In this section we show the variation of the number of $K\alpha$ photons vs. the thickness of the CHCl overlayer. Fig.7 shows the case of the thick Cu targets.

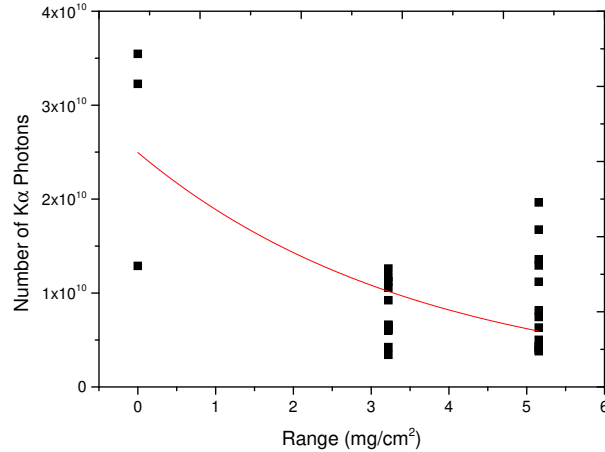


FIG. 7. Number of $K\alpha$ photons vs. range of CHCl for thick Cu targets at 3ω . Data points are interpolated with an exponential function.

With increasing the CHCl thickness the $K\alpha$ signal is decreasing. From such decrease we can evaluate the average energy of HE as we will do in the next section.

We repeated the analysis for thin multilayer targets, Fig.8.

While Fig.7 shows a clear decrease, fig.8 shows a quasi flat behaviour. The two might not necessary be in contradiction because Fig.7 extends to larger CHCl thickness so it allows to better see any decrease. In addition in Fig.8, the decreasing slope could be probably hidden inside the large shot-to-shot fluctuations and the low statistics.

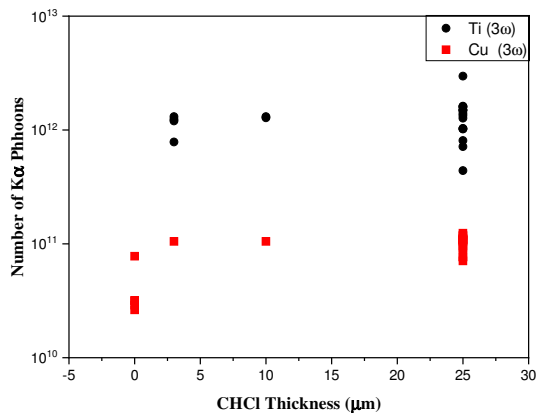


FIG. 8. Number of $K\alpha$ photons vs. CHCl thickness for thin targets at 3ω .

With respect to Fig.8 we also notice that the number of Cu $K\alpha$ photons emitted from pure Cu targets (no overlayer) is less than that obtained when the plastic overlayer is present. This is indeed expected when the laser beam directly interact with Cu, since it produces a hot ablated plasma where Cu is strongly ionized and emit thermal X-ray or shifted $K\alpha$ lines instead of cold $K\alpha$ line which is collected by crystal.

IV. ESTIMATION OF HOT ELECTRON AVERAGE ENERGY

A. Exponential interpolation

The data of Fig.7 can be interpolated with an exponential function,

$$N_e(x) = N_0 \exp(-x/R) \quad (2)$$

where N_0 is the number of photons which would ideally be emitted from a target without overlayer and x the areal density before the tracer layer¹⁴. By assuming that the number of emitted $K\alpha$ photons is roughly proportional to the number of HE reaching the tracer layer, we can estimate the range (g/cm^2), R , of HE. This is a crucial parameter since shows how much HE can penetrate into the target and hence allows to estimate their average energy. For this purpose we can use the ESTAR database which relates the initial energy of HE to range⁸. The simplest way to evaluate HE energy is assuming a mono energetic electron beam instead of considering a realistic electron energy distribution (i.e. all of HE have the same energy corresponding to the average energy in the distribution) and assuming that all electrons travel in straight lines (instead of realistic trajectories characterized by scattering and angular divergence).

For thick targets, Fig.7, we fitted the curve with an exponential function, Eq. 2, which gives the initial number of photons $N_0 = (2.5 \pm 0.3) \times 10^{10}$ and a range $R = 3.6 \pm 0.6$ (mg/cm^2). According to the ESTAR database such range corresponds to HE with energy $T_{HE} \approx 41.5 \pm 6$ keV.

For thin targets, the number of $K\alpha$ photons doesn't seem to change appreciably with increasing the plastic thickness from 3 to 25 μm . Hence, we can't evaluate energy of HE with the same method. For these targets we use a different approach based on the ratio of the number of $K\alpha$ photons of Ti to the number of $K\alpha$ photons of Cu vs. CHCl thickness. Fig.9 shows that, taking into account the very large shot-to-shot fluctuations, the ratio (Ti $K\alpha$ /Cu $K\alpha$) can be assumed to be constant and $\approx 12 \pm 7$.

In the following, we assume the ratio of $K\alpha$ photons is equal to the ratio of the number

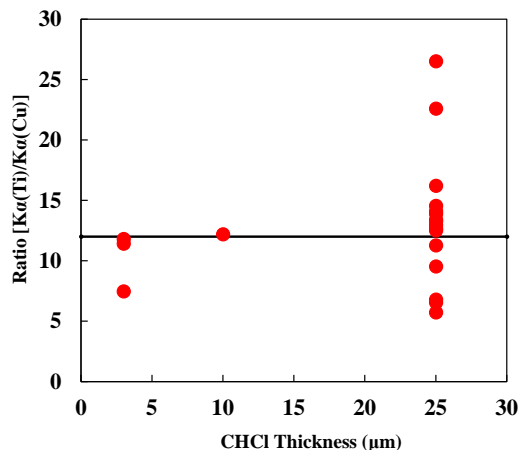


FIG. 9. Ratio of the number of $K\alpha$ photons of Ti to the number of $K\alpha$ photons of Cu vs. CHCl thickness for thin targets at 3ω . The solid line represents the average ratio.

of electrons which arrive to the Ti layer to those arrive to the Cu layer. The number of electrons reaching the Ti layer is

$$N_{Ti,0} = N_0 \exp\left(-\frac{l_{CH}}{R_{CH}(E_0)}\right) \quad (3)$$

where N_0 is the initial number of electrons, l_{CH} is the CHCl areal density and $R_{CH}(E_0)$ is the range in CHCl which is a function of energy and E_0 is the initial energy of HE (again assumed mono energetic). The ESTAR database also gives the energy loss, ΔE_{CHCl} , in the CHCl layer. Accordingly, electrons with initial energy E_0 arrive to the Ti layer with energy $E_{Ti} = E_0 - \Delta E_{CHCl}$. We assume on average the Ti $K\alpha$ photons are emitted at half of the Ti layer

$$N_{Ti} = N_{Ti,0} \exp\left(-\frac{l_{Ti}/2}{R_{Ti}(E_{Ti})}\right) \quad (4)$$

where l_{Ti} is the areal density of the Ti layer and $R_{Ti}(E_{Ti})$ is the range in Ti for electrons with energy E_{Ti} .

The fraction of more energetic electrons of $N_{Ti,0}$ which pass Ti layer and reach the Cu layer is given by

$$N_{Cu,0} = N_{Ti,0} \exp\left(-\frac{l_{Ti}}{R_{Ti}(E_{Ti})}\right) \quad (5)$$

They reach the Cu layer with an energy $E_{Cu} = E_{Ti} - \Delta E_{Ti}$ where ΔE_{Ti} is the energy loss in Ti layer. For the Cu layers we assume that on average Cu $K\alpha$ photons are emitted at the depth equal to $R_{Cu}/2$, where $R_{Cu}(E_{Cu})$ is the range in Cu for electrons with energy E_{Cu} . Hence we have

$$N_{Cu} = N_{Cu,0} \exp\left(-\frac{R_{Cu}(E_{Cu})/2}{R_{Cu}(E_{Cu})}\right) \approx 0.6 \times N_{Cu,0} \quad (6)$$

accordingly the ratio equals to

$$\frac{N_{Ti}}{N_{Cu}} = 1.7 \times \exp\left(\frac{l_{Ti}/2}{R_{Ti}(E_{Ti})}\right) \quad (7)$$

which depends on the initial energy of HE(E_0), the areal density of the CHCl layer ($E_{Ti} = E_0 - \Delta E_{CHCl}$) and the areal density of the Ti layer ($E_{Cu} = E_0 - \Delta E_{CHCl} - \Delta E_{Ti}$). Also the number of emitted $K\alpha$ photons is proportional to

$$N(K\alpha) \approx N \sigma(E) n \omega_K l \quad (8)$$

where N is the number of HE with energy sufficient to generate $K\alpha$ emissions, l (cm) is the thickness of each layer, ω_K is the florescence yield of K shell which for Cu is $\omega_{(K,Cu)} = 0.38$ and for Ti is $\omega_{(K,Ti)} = 0.17$, n (cm^{-3}) is the ion density which for Cu is $n_{Cu} = 8.4 \times 10^{22} cm^{-3}$ and for Ti is $n_{Ti} = 5.7 \times 10^{22} cm^{-3}$. The $K\alpha$ cross section, σ (cm^2), is energy dependent and given by¹⁵

$$\sigma(E)(cm^2) = 7.92 \times 10^{-14} \frac{1}{EE_K} \ln\left(\frac{E}{E_K}\right) \quad (9)$$

where E is the energy of HE (in eV) and E_K is the $K\alpha$ ionization energy which for Cu is about 8987 eV. Since the CHCl thickness varies and σ is energy dependent we calculate its values depending on the HE energy. In general, we find for Cu, $\sigma_{Cu} \approx (2 - 4) \times 10^{-22} cm^2$ and for Ti, $\sigma_{Ti} \approx (8 - 9) \times 10^{-22} cm^2$.

Finally the ratio is proportional to

$$\frac{N(K\alpha)_{Ti}}{N(K\alpha)_{Cu}} \approx \frac{N_{Ti}}{N_{Cu}} \times \frac{\sigma_{Ti} n_{Ti} \omega_{k,Ti} l_{Ti}}{\sigma_{Cu} n_{Cu} \omega_{k,Cu} L_{Cu}} \quad (10)$$

where L_{Cu} is the penetration depth in Cu layer. Table.I summarises the results.

TABLE I. Ratio of the number of $K\alpha$ photons of Ti to the number of $K\alpha$ photons of Cu following Eq.10. $l_{CHCl} = 10\mu m$ is chosen for this analysis.

E (keV)	R_{CH} (mg cm^{-2})	ΔE (keV)	E_{Ti} (keV)	R_{Ti} (mg cm^{-2})	$N_{Ti,0}$	$\frac{\sigma_{Ti}}{(10^{-22})}$ (cm^2)	N_{Ti}	ΔE_{Ti} (keV)	E_{Cu} (keV)	$N_{Cu,0}$	R_{Cu} (mg cm^{-2})	$\frac{\sigma_{Cu}}{(10^{-22})}$ (cm^2)	N_{Cu}	$\frac{N_{Ti}}{N_{Cu}}$
40	3.2	9.3	30.7	2.8	0.67	11.6	0.44	29.1	1.6	0.20	0	0	0	0
50	4.7	7.9	42.1	4.8	0.76	9.5	0.62	23.2	18.9	0.39	1.3	2.6	0.24	19.2
52	5.0	7.7	44.3	5.2	0.77	9.1	0.65	22.4	22	0.42	1.7	3.0	0.25	11.6
54	5.4	7.5	46.5	5.7	0.79	8.8	0.67	21.7	24.9	0.45	2.1	3.3	0.27	8.0

The analysis estimate HE energy about $T_{HE} \approx 52_{-5}^{+9}$ keV. Taking into account the error bars, this result is comparable with what obtained from Fig.7.

B. Harrach-Kidder model

In this section we estimate the HE energy using the semi-analytical model developed by Harrach & Kidder⁷.

The advantage of H-K model with respect to other analytical models^{16,17} is that these models don't apply to targets with low atomic number while H-K model not only benefits from simple analytical formula (which give better physical intuition) but also can be used for materials with any atomic numbers. More importantly its predictions are in good agreement with the experimental results for low HE energy⁷.

In the model, the HE source is planar, isotropic and characterized by a Maxwellian velocity distribution with temperature T_{HE} . A fraction of HEs penetrate directly towards the dense target and deposit their energy which is calculated using Spencer energy deposition function¹⁸. The energy deposited at distance z into the target is proportional to

$$N(z) \approx N_0 \exp[-\beta \sqrt{z/R}] \quad (11)$$

where N_0 is the initial number of electrons and β is a parameter which characterizes the propagating material, R is the range and z is the distance travelled inside the target in normal direction to the surface. Both R and z are measured in (g/cm^2) unit. The relation between the range and HE temperature, T_{HE} , is

$$R = b(T_{HE})^{1+\mu} \quad (12)$$

where T_{HE} in (keV) and parameters b and μ depend on the propagating material. To apply Eqs.11 and 12, we need to know the values of β , b , and μ . We choose the values of carbon: $\beta_{CHCl}=1.85$, $b_{CHCl}=4.6 \times 10^{-6}$, and $\mu_{CHCl}=0.78^7$. This choice is justified by the fact that in the plastic layer, in front of the target, where HE generated and propagated, mostly carbon atoms are responsible for the HE stopping power¹⁹.

In the following we consider only thick Cu targets. In order to apply H-K model we should convert the thickness of the thick targets (CH+Cu) to the equivalent total areal density (g/cm^2) as needed in Eq.11. To do that we multiply the length of each layer, $l(cm)$, to its density, $\rho(g/cm^3)$. We have

$$z(mg/cm^2) = (l_{CH} \times \rho_{CH}) + (l_{Cu} \times \rho_{Cu}) \quad (13)$$

where $\rho_{CHCl}=1.289 (g/cm^3)$ and $\rho_{Cu}=8.92 (g/cm^3)$. For CHCl layer we have $l_{CHCl} = 0, 25, \text{ and } 40 \mu m$. Unfortunately l_{Cu} is not defined for the thick targets which means we have to do some assumptions for l_{Cu} . According to Sec.IV A, the maximum energy of HE is about 52_{-5}^{+9} keV as estimated by the ratio analysis. It means the maximum energy of HE should be about 60 keV. By looking to the ESTAR database for the Cu element, 60 keV equals to range $R=9.46 mg/cm^2$ which corresponds to a penetration depth ($L=R/\rho_{Cu}$) of $L=10 \mu m$ into the Cu layer. Hence, $10 \mu m$ should be a reasonable choice for the thickness of the Cu layer for thick targets. Now we can assume that X-ray Cu $K\alpha$ photons are emitted on average at half of this distance, i.e. $l_{Cu} = 5 \mu m$. Substituting in Eq.13 gives $z(mg/cm^2) = 4.45, 7.7, \text{ and } 9.7$ for $l_{CHCl} = 0, 25, \text{ and } 40 \mu m$ respectively. Now we can plot the number of $K\alpha$ photons vs the total length of the target as presented in Fig. 10. Fitting according to Eq.11 allows to find the range, $R (g/cm^2)$ and from this we can find the HE temperature using Eq.12.

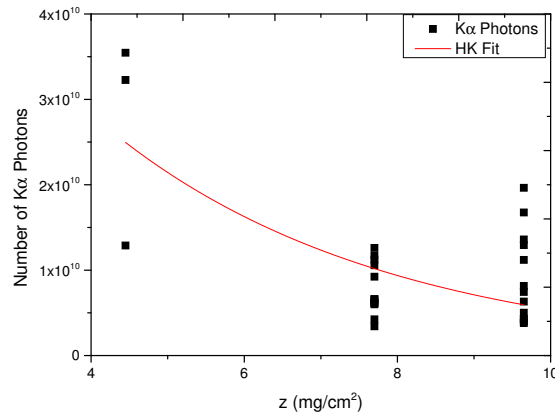


FIG. 10. Number of $K\alpha$ photons vs the total areal density of target (Eq.13) and its fit according to H-K model (Eq.11).

For $l_{Cu} = 5 \mu m$, the analyses show $N_0 = (5.0 \pm 3.0) \times 10^{11}$ and $R = 1.7 \pm 0.6 mg/cm^2$ which

corresponds to HE with energy $T_{HE} = 27.7 \pm 5$ keV.

We can also choose different values for Cu layer thickness such as $l_{Cu} = 2.5$ and $1 \mu m$ to see which HE temperature is estimated by the H-K model. For $l_{Cu} = 2.5 \mu m$ we have $N_0 = (1.4 \pm 0.5) \times 10^{11}$ and $R = 2.7 \pm 0.9 \text{ mg/cm}^2$ which corresponds to HE with energy $T_{HE} = 35.9 \pm 6.3$ keV. For $l_{Cu} = 1 \mu m$ we have $N_0 = (0.6 \pm 0.1) \times 10^{11}$ and $R = 4.1 \pm 1.3 \text{ mg/cm}^2$ which corresponds to HE with energy $T_{HE} = 45.4 \pm 7.6$ keV. We have to mention for $l_{Cu} \leq 0.5 \mu m$, H-K model gives very unrealistic high HE temperature. Accordingly, the maximum HE temperature estimated with the H-K model is less than $\leq 45.4 \pm 7.6$ keV.

HE energy estimated above by the H-K model are according to the values of μ , β , and b parameters for the Carbon element. For the thick Cu targets without CH front layer, it is instructive to see which T_{HE} is estimated by the H-K model when we use parameters relevant to the Cu element in Eqs.11 and 12. In Harrach & Kidder paper⁷, the values of μ , β , and b parameters are defined only for C, Al, and Au elements. To find the value of each parameter, we use a function which fits the best to the values of C, Al, and Au elements and by interpolating we estimate the value of that parameter for the Cu element. The analysis shows the function which fits the best to the data for all three parameters is a power function in the form of ax^c where a and c should be defined. For μ , we find $a=0.93$ and $c=-0.1$ which gives $\mu_{Cu} = 0.668$. For b we find $a=1.63$ and $c=0.56$ which gives $b_{Cu} = 10.8 \times 10^{-6}$. For β we find $a=1.2$ and $c=0.23$ which gives $\beta_{Cu} = 2.63$.

For $l_{Cu} = 5 \mu m$ and considering the values relevant to Cu in H-K model, the analyses show the same initial number of photons, i.e. $N_0 = (5.0 \pm 3.0) \times 10^{11}$, but the range, now, is $R = 3.4 \pm 1.2 \text{ mg/cm}^2$ which corresponds to HE with temperature $T_{HE} = 31.6 \pm 6$ keV which is not too different from the prediction using carbon values in H-K model for $l_{Cu} = 5 \mu m$.

The advantage of H-K model to the simple exponential fit used in Sec.IV A is that the simple exponential gives only a single HE energy as an average of whole HE population assuming energetic electrons travelling in forward straight trajectories. Instead, the H-K model includes phenomena such as straggling of electron trajectories and the back reflection of a part of the electrons from the tracer layers. Moreover the H-K model describes the propagation of HE with moderate energies in matter which are strongly affected by the collisions and therefore quickly get a quasi isotropic propagation.

Overall, by looking to N_0 estimated for $l_{Cu} = 2.5$ and $5 \mu m$, we can see they are much higher than the experimental initial number of photons which are less than 4×10^{10} , Fig. 10, while N_0 estimated with $l_{Cu} = 1 \mu m$ is close to the experimental data and also to the one estimated with the ESTAR database. Hence, it seems $T_{HE} = 45.4 \pm 7.6$ keV represents more precisely the HE temperature.

Our measurements are in agreements with the previous experimental results and the results of other groups obtained in experiment with similar intensities at OMEGA laser facility where they found $T_{HE} \approx 30$ keV²⁰.

V. CONVERSION EFFICIENCY

Finally we estimate the conversion efficiency, η , i.e. the total energy in HE, E_{HE} , with respect to the incident laser energy, E_{laser}

$$\eta = \frac{E_{HE}}{E_{laser}} \quad (14)$$

E_{HE} is equal to $N_{e0} \times T_{HE}$, where N_{e0} is the total number of HE initially produced inside the target and T_{HE} is the average energy of HE. The number of electrons, N_{e0} , is related to the number of emitted $K\alpha$ photons by Eq.8, i.e.

$$N_{e0} \approx \frac{N_0}{\omega_K \sigma n_{Cu} l_{Cu}} \quad (15)$$

Here, for sake of brevity, we assume mono energetic electrons and we perform the calculation

of conversion efficiency with reference only to Cu $K\alpha$ photons. Hence, $\omega_K = 0.44$, $n_{Cu} = 8 \times 10^{22} \text{cm}^{-3}$, and $\sigma = 2 \times 10^{-22} \text{cm}^2$. Following H-K model, Eq.11, for $l_{Cu} = 1 \mu\text{m}$, we have $T_{HE} = 45.4 \pm 7.6 \text{ keV}$ and $N_0 = (0.6 \pm 0.1) \times 10^{11}$. Considering the maximum laser energy $E_{laser} \approx 170 \text{ J}$, Eq.14 gives $\eta \approx 0.36 \pm 0.6 \%$.

This result is in good agreement with the estimation of similar experiment²¹. They are also in fair agreement with the results of detailed Monte Carlo simulations $\eta \approx 0.14 \pm 0.1 \%$ ²².

VI. CONCLUSION

We performed an experiment to characterize HE produced in laser-plasma interaction at intensities relevant to SI. We used two types of targets during the experiment for HE studies: thin multilayer targets and thick Cu targets.

For thick targets we followed two approaches: first we used an exponential fit to infer HE penetration in target and compared this with data from the ESTAR database. Second we used the model developed by Harrach-Kidder. The two approaches give $T_{HE,exp} = 41.5 \pm 6 \text{ keV}$ and $T_{HE,HK} \leq 45.4 \pm 7.6 \text{ keV}$ respectively.

For the thin multilayer targets, we estimated the temperature of HE from the ratio of the number of $K\alpha$ photons of Ti to the number of $K\alpha$ photons of Cu. This analysis estimated HE energies $\approx 52 \pm 5 \text{ keV}$. This value compares well to $41.5 \pm 6 \text{ keV}$. In both cases the basic assumption is replacing the HE distribution with monoenergetic electrons. Instead H-K calculations refer to a Maxwellian distribution.

In conclusion from our experiment we see that using 3ω irradiation of low Z targets at intensities of interest for shock ignition, we generate a HE distribution with $\eta \leq 1\%$ and $T_{HE} \leq 45.4 \text{ keV}$. Although this is low, still there is a significant number of electrons with $E > 100 \text{ keV}$ in a Maxwell distribution with this temperature. The effect of such HE production in the context of shock ignition must be therefore carefully considered in future works.

ACKNOWLEDGMENTS

This work has been carried out within the framework of the EUROfusion Enabling Research Project: AWP17-ENR-IFE-CEA-01 *Preparation and Realization of European Shock Ignition Experiments* and has received funding from the Euratom research and training programme 2014-2018 under grant agreement No.633053. The views and opinions expressed herein do not necessarily reflect those of the European Commission.

¹R. Betti, C. D. Zhou, K. S. Anderson, L. J. Perkins, W. Theobald, and A. A. Solodov, “Shock ignition of thermonuclear fuel with high areal density,” *Phys. Rev. Lett.* **98**, 155001 (2007).

²D. Batani, S. Baton, A. Casner, S. Depierreux, M. Hohenberger, O. Klimo, M. Koenig, C. Labaune, X. Ribeyre, C. Rousseaux, G. Schurtz, W. Theobald, and V. Tikhonchuk, “Physics issues for shock ignition,” *Nuclear Fusion* **54**, 054009 (2014).

³L. J. Perkins, R. Betti, K. N. LaFortune, and W. H. Williams, “Shock ignition: A new approach to high gain inertial confinement fusion on the national ignition facility,” *Phys. Rev. Lett.* **103**, 045004 (2009).

⁴X. Ribeyre, G. Schurtz, M. Lafon, S. Galera, and S. Weber, “Shock ignition: an alternative scheme for hiper,” *Plasma Physics and Controlled Fusion* **51**, 015013 (2009).

⁵P. Koester, L. Antonelli, S. Atzeni, J. Badziak, F. Baffigi, D. Batani, C. A. Cecchetti, T. Chodukowski, F. Consoli, G. Cristoforetti, R. D. Angelis, G. Folpini, L. A. Gizzi, Z. Kalinowska, E. Krouscky, M. Kucharik, L. Labate, T. Levato, R. Liska, G. Malka, Y. Maheut, A. Marocchino, P. Nicolai, T. O’Dell, P. Parys, T. Pisarczyk, P. Raczka, O. Renner, Y. J. Rhee, X. Ribeyre, M. Richetta, M. Rosinski, L. Ryc, J. Skala, A. Schiavi, G. Schurtz, M. Smid, C. Spindloe, J. Ullschmied, J. Wolowski, and A. Zaras, “Recent results from experimental studies on laserplasma coupling in a shock ignition relevant regime,” *Plasma Physics and Controlled Fusion* **55**, 124045 (2013).

⁶D. Batani, G. Malka, G. Schurtz, X. Ribeyre, E. Lebel, L. Giuffrida, V. Tikhonchuk, L. Volpe, A. Patria, P. Koester, L. Labate, L. A. Gizzi, L. Antonelli, M. Richetta, J. Nejd, M. Sawicka, D. Margarone, M. Krus, E. Krouscky, J. Skala, R. Dudzak, A. Velyhan, J. Ullschmied, O. Renner, M. Smid, O. Klimo, S. Atzeni, A. Marocchino, A. Schiavi, C. Spindloe, T. O’Dell, T. Vinci, J. Wolowski, J. Badziak, T. Pisarczyk, M. Rosinski, Z. Kalinowska, and T. Chodukowski, “Preliminary results from recent experiments and future roadmap to shock ignition of fusion targets,” *Journal of Physics: Conference Series* **399**, 012005 (2012).

- ⁷R. J. Harrach and R. E. Kidder, “Simple model of energy deposition by suprathermal electrons in laser-irradiated targets,” *Phys. Rev. A* **23**, 887–896 (1981).
- ⁸“Estar database,” <http://www.nist.gov/pml/data/star/index.cfm> (2005).
- ⁹D. Batani, L. Antonelli, S. Atzeni, J. Badziak, F. Baffigi, T. Chodukowski, F. Consoli, G. Cristoforetti, R. De Angelis, R. Dudzak, G. Folpini, L. Giuffrida, L. A. Gizzi, Z. Kalinowska, P. Koester, E. Krousky, M. Krus, L. Labate, T. Levato, Y. Maheut, G. Malka, D. Margarone, A. Marocchino, J. Nejdil, P. Nicolai, T. O’Dell, T. Pisarczyk, O. Renner, Y. J. Rhee, X. Ribeyre, M. Richetta, M. Rosinski, M. Sawicka, A. Schiavi, J. Skala, M. Smid, C. Spindloe, J. Ullschmied, A. Velyhan, and T. Vinci, “Generation of high pressure shocks relevant to the shock-ignition intensity regime,” *Physics of Plasmas* **21**, 032710 (2014), <http://dx.doi.org/10.1063/1.4869715>.
- ¹⁰N.-L. F. A Ridgeley, “A comparison of kodak def industrex cx and industrex ax films at soft x-ray wavelengths,” (1989).
- ¹¹O. Renner, M. Šmíd, D. Batani, and L. Antonelli, “Suprathermal electron production in laser-irradiated cu targets characterized by combined methods of x-ray imaging and spectroscopy,” *Plasma Physics and Controlled Fusion* **58**, 075007 (2016).
- ¹²M. Šmíd, O. Renner, F. B. Rosmej, and D. Khaghani, “Investigation of x-ray emission induced by hot electrons in dense cu plasmas,” *Physica Scripta* **2014**, 014020 (2014).
- ¹³T. Pisarczyk, S. Gus’kov, O. Renner, N. Demchenko, Z. Kalinowska, T. Chodukowski, M. Rosinski, P. Parys, M. Smid, J. Dostal, and et al., “Pre-plasma effect on laser beam energy transfer to a dense target under conditions relevant to shock ignition,” *Laser and Particle Beams* **33**, 221236 (2015).
- ¹⁴A. Morace and D. Batani, “Spherically bent crystal for X-ray imaging of laser produced plasmas,” *Nuclear Instruments and Methods in Physics Research A* **623**, 797–800 (2010).
- ¹⁵L. D. Landau and E. M. Lifshitz, *Quantum mechanics: non-relativistic theory*, Vol. 3 (Elsevier, 2013) Chap. XVIII.
- ¹⁶G. J. Caporaso and S. S. Wilson, Lawrence Livermore National Laboratory Report No. UCRL 83308 (unpublished) (1979).
- ¹⁷Y. Lee and R. T. Trainor, Lawrence Livermore National Laboratory Report No. UCID-18574-79-4 pp.34-41 (unpublished) (1980).
- ¹⁸L. Spencer, National Bureau of Standards Monograph 1 (unpublished) (1959).
- ¹⁹D. Batani, J. R. Davies, A. Bernardinello, F. Pisani, M. Koenig, T. A. Hall, S. Ellwi, P. Norreys, S. Rose, A. Djaoui, and D. Neely, “Explanations for the observed increase in fast electron penetration in laser shock compressed materials,” *Phys. Rev. E* **61**, 5725–5733 (2000).
- ²⁰W. Theobald, R. Nora, M. Lafon, A. Casner, X. Ribeyre, K. S. Anderson, R. Betti, J. A. Delettrez, J. A. Frenje, V. Y. Glebov, O. V. Gotchev, M. Hohenberger, S. X. Hu, F. J. Marshall, D. D. Meyerhofer, T. C. Sangster, G. Schurtz, W. Seka, V. A. Smalyuk, C. Stoeckl, and B. Yaakobi, “Spherical shock-ignition experiments with the 40 + 20-beam configuration on omega,” *Physics of Plasmas* **19**, 102706 (2012), <http://dx.doi.org/10.1063/1.4763556>.
- ²¹S. Y. Gus’kov, S. Borodziuk, M. Kalal, A. Kasperczuk, V. N. Kondrashov, J. Limpouch, P. Pisarczyk, T. Pisarczyk, K. Rohlena, J. Skala, and J. Ullschmied, “Investigation of shock wave loading and crater creation by means of single and double targets in the pals-laser experiment,” *Journal of Russian Laser Research* **26**, 228–244 (2005).
- ²²e. a. Batani D., Antonelli L., “Progress in understanding the role of hot electrons for the shock ignition approach to inertial confinement fusion,” *Nuclear Fusion*, submitted (2018).
- ²³J. P. Santos, F. Parente, and Y.-K. Kim, “Cross sections for k-shell ionization of atoms by electron impact,” *Journal of Physics B: Atomic, Molecular and Optical Physics* **36**, 4211 (2003).
- ²⁴D. Batani, M. Koenig, S. Baton, F. Perez, L. A. Gizzi, P. Koester, L. Labate, J. Honrubia, L. Antonelli, A. Morace, L. Volpe, J. Santos, G. Schurtz, S. Hulin, X. Ribeyre, C. Fourment, P. Nicolai, B. Vauzour, L. Gremillet, W. Nazarov, J. Pasley, M. Richetta, K. Lancaster, C. Spindloe, M. Tolley, D. Neely, M. Kozlov, J. Nejdil, B. Rus, J. Wolowski, J. Badziak, and F. Dorchies, “The hiper project for inertial confinement fusion and some experimental results on advanced ignition schemes,” *Plasma Physics and Controlled Fusion* **53**, 124041 (2011).